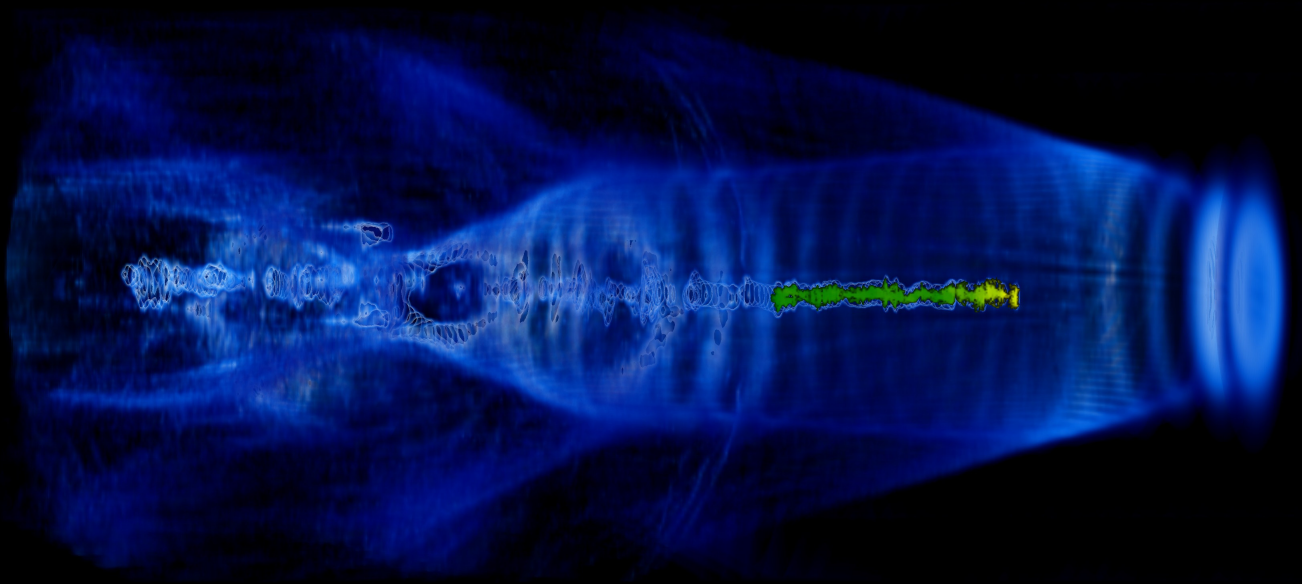


MASTER'S THESIS 2019

A compact plasma beam dump for next generation particle accelerators

OSCAR JAKOBSSON

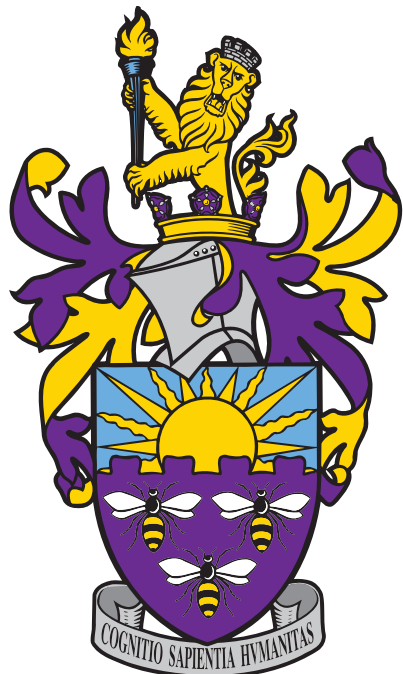


SCHOOL OF PHYSICS AND ASTRONOMY
THE UNIVERSITY OF MANCHESTER



A compact plasma beam dump for next generation particle accelerators

OSCAR JAKOBSSON



School of Physics and Astronomy
Cockcroft Accelerator Group
THE UNIVERSITY OF MANCHESTER
Manchester, United Kingdom 2019

A compact plasma beam dump for next generation particle accelerators
OSCAR JAKOBSSON

© OSCAR JAKOBSSON, 2017.

Supervisor: Guoxing Xia, Cockcroft Accelerator Group

Master's Thesis 2019
School of Physics and Astronomy
Cockcroft Accelerator Group
The University of Manchester

Cover: XXX.

Typeset in L^AT_EX

A compact plasma beam dump for next generation particle accelerators

OSCAR JAKOBSSON

School of Physics and Astronomy

The University of Manchester

Abstract

Lore ipsum dolor sit amet, consectetur adipisicing elit, sed do eiusmod tempor incididunt ut labore et dolore magna aliqua. Ut enim ad minim veniam, quis nostrud exercitation ullamco laboris nisi ut aliquip ex ea commodo consequat. Duis aute irure dolor in reprehenderit in voluptate velit esse cillum dolore eu fugiat nulla pariatur. Excepteur sint occaecat cupidatat non proident, sunt in culpa qui officia deserunt mollit anim id est laborum.

Keywords: Plasma wakefield acceleration, deceleration, beam dump, ILC, EuPRAXIA

Acknowledgements

 Lorem ipsum dolor sit amet, consectetur adipisicing elit, sed do eiusmod tempor incididunt ut labore et dolore magna aliqua. Ut enim ad minim veniam, quis nostrud exercitation ullamco laboris nisi ut aliquip ex ea commodo consequat. Duis aute irure dolor in reprehenderit in voluptate velit esse cillum dolore eu fugiat nulla pariatur. Excepteur sint occaecat cupidatat non proident, sunt in culpa qui officia deserunt mollit anim id est laborum.

Oscar Jakobsson, Manchester, January 2019

Contents

List of Figures	xi
1 Introduction	1
1.1 Conventional accelerators	1
1.2 Plasma wakefield accelerators	2
1.3 Beam dumps	2
1.4 Outline of report	4
2 Theoretical foundations	5
2.1 Introduction	5
2.2 Linear fluid model	5
2.2.1 Longitudinal Accelerating Field	7
2.2.2 Transverse Focusing Field	10
2.3 Non-linear Regime	12
2.3.1 Wave-breaking field	12
2.4 Particle interactions with matter	15
2.4.1 Bohr-Fermi-Bethe-Bloch Theory	15
2.4.2 Collective Plasma Deceleration – Non-Linear regime	15
2.4.3 Collective Plasma Deceleration – Linear regime	16
2.4.4 Notes Bonatto	18
3 Simulations	19
3.1 Plasma simulations	19
3.2 Particle-in-Cell Codes	20
3.3 EPOCH	21
3.3.1 Input deck	21
3.3.2 Non-analytical bunch initialisation	22
3.4 Notes.	23
4 Simulation tests	25
4.1 Plasma deceleration - Uniform density	25
4.1.1 Transverse instabilities in quasilinear regime	25
4.2 Hybrid Scheme - Feasibility study	25
4.2.1 Initialising a decelerated bunch	25
4.2.2 Introduction of co-propagating laser	25
5 Ongoing and future work	27

Contents

6 Conclusion	29
Bibliography	31
A Appendix: Input decks	I

List of Figures

1.1	3
2.1	Simulation vs. theory for linear regime with $n_p/n_b = 100$	10
2.2	Plot corresponding to Dawson's derivation of the wave-breaking field [ref. Sahai].	14
2.3	Non-linear regime, plasma density perturbations. Added custom legend with density=number of electrons / grid-square size.	16
2.4	Should these three plots be in results or here? OR PUT SIMUALTIONS CHAPTER BEFORE THEORY CHAPTER. Then theory can be used to also verify that simulations work. Probably not, better explain everything to motivate what simulations to be done	17

List of Figures

1

Introduction

1.1 Conventional accelerators

An estimated 30 000 particle accelerators are currently in operation worldwide, providing beams of high-energy particles for science and industry. For instance, monoenergetic electron bunches allows for the generation of high-quality X-ray pulses through the use of undulators; a technique by which high-energy electron bunches are rapidly oscillated back-and-forth perpendicular to their direction of propagation. This oscillatory motion can generate highly coherent synchrotron radiation in the X-ray spectrum using ultra-relativistic electrons , which can be used in medicine for advanced tissue diagnostics (something tomography) (add length) . Operating at higher energies, the 1.7 km long European free electron laser (XFEL) facility in Hamburg, Germany, uses 17.5 GeV electron bunches to generate ultra short, extremely brilliant X-ray pulses which are used for fundamental research into the structure proteins, molecules..and even create movies of molecular motion [1]. Probing even smaller length scales takes us into the realm of high-energy physics, where the size of the accelerators grows accordingly. From the ... long SLAC Linear Colider (SLC) at Fermilab to the Large Electron Positron colider (LEP) which accelerated electrons and positrons up to 100 GeV and now named the LHC accelerates protons to 14TeV, the fine details of the smallest constituents of our theories is being explored through tests of the standard model. Even more energetic accelerators, such as the International Linear Collider (ILC) will push the particle energies even higher. However, as energy increases, the size of the accelerator increase as well.

The reason for this increase stems from the method by which particles are accelerated. High-energy particle accelerators rely on resonant radiofrequency (RF) cavities. These are evacuated cavities which the particle beam passes through. The design and operation of these cavities are carefully engineered so as to set up an oscillating electric potential which acts to accelerate and squeeze the particle bunches together. The current RF cavities at the LHC privde an accelerating field of 5MV/m, such that the energy gain per meter is 5MeV. Hence, to reach TeV energies the protons at the LHC needs to pass through tens of millions RF cavities, which clearly necessitates a circular accelerator. The large size of the LHC then comes from the fact that the bending of the particles around the circular accelerator is limit by the magnetic field strength and the emission of synchrotron radiation. [Add how much more energy LEP would have required to find the higgs]. Even if one used a combination of circular accellerators feed into a linear accelerator to avoid synchrotron energy loss, as in the proposed ILC, the size would still need to be large given that the maximum electric acceleration field in an RF cavity is 100MV/m, beyond which point....rf breakdown (seperation of ions and electrons). Clearly, even if the particle physics community is granted ever increasing particle accelerators, as the demand for GeV particle accelerators

grows in medicine, industry and fundamental research, the size and cost of accelerators is and will continue to be a limit factor to future progress if no other means of acceleration is possible.

1.2 Plasma wakefield accelerators

Several novel accelerators techniques exists in various stages of development. The most widespread of these is based on the phenomena of *plasma wakefield acceleration*. Driving a relativistic particle beam or a high intensity laser pulses through a preformed plasma can excite waves in the plasma with phase velocities equal to the group velocity of the particle or laser driver [Plasma Wakefield Acceleration for Ultrahigh-Energy Cosmic Rays]. The waves, or "wakefields", are large-amplitude oscillations of the plasma-electron density behind the driver which are able to support accelerating fields of hundreds of GV/m; thousands of times higher than conventional RF cavities. By injecting an electron, or positron, bunch behind the driver one can then achieve constant acceleration by effectively letting the particle bunch surf the plasma-electron wave. In this manner, huge energy gains can be achieved over relatively short propagation distances if a sufficiently powerful driver is available. In fact, in this form of plasma enabled acceleration was proposed in 1979 by Tajima and Dawson [], not only as a viable terrestrial particle accelerator but also as a generation mechanism of ultrahigh-energy cosmic rays in the plasma rich environment around newly formed pulsars. At this point in time the lack of sufficiently high intensity lasers was a limit factor in exploring these ideas experimentally. The invention of the chirped-pulse amplification techniques for lasers in the 1980s by Strickland and Mourou ¹[] gave researchers access to ultrashort high-intensity laser pulses. This opened up the possibility of laser driven plasma wakefield acceleration and several experiments followed [Kieran's thesis].**Iwfa, then pwfa, FACET,DESY,AWAKE** These experiments are paving the way towards compact high-energy particle accelerators at GeV energies with great promise to science and industry. One can also imagine a future in which plasma wakefield accelerators are used in high-energy physics, perhaps in conjugation with conventional accelerators as a pre-accelerator [?] or as an energy booster. Even though the latter is probably decades away, both GeV and TeV accelerators might still be able to benefit from plasma wakefield phenomena. Regardless of the means of acceleration, be it larger conventional accelerators or smaller plasma wakefield accelerators, the ultra-relativistic beams produced will need to be dealt with. The current approach for both small and large accelerators is to dump the energy of the beam.

1.3 Beam dumps

When in operation, the 100 GeV electron and positron beams at the LEP at CERN were expanded, to decrease the intensity, and directed into a 2 m long, 40 cm in diameter, aluminium alloy block in order to be brought to a stop [2]. The proposed water-based beam dump for the ILC [3], which is to operate at 500 GeV, is significantly different to its lower energy predecessor at LEP. The increased energy and intensity of the ILC beam makes the extraction of its energy from a solid material beam dumps exceedingly difficult because of the limitations imposed by thermal conduction [Design of an 18 MW]. By using a ... m³ tank of water the ILC beam energy can be deposited and removed using a pumping system. The high intensity beams however lead to water temperatures in excess of 150°C, resulting in

¹2018 Nobel prize

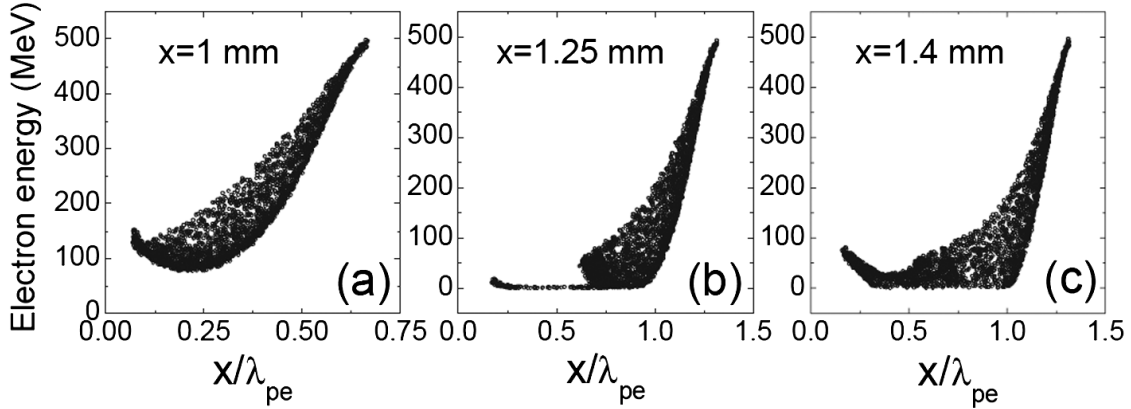


Figure 1.1

...(catalysis?) of water into hydrogen and oxygen gas. This necessitates a safe and efficient way to remove and store these gases. Furthermore, the beam interaction with the water molecules will create the radioactive nuclei Be7 and..., this requires a waste-water storage tank which will need to be treated. The tank itself will also suffer radiation damages, specifically the window through which the beam enters the vessel. A report by ...et al. [3] estimates that this window will need to be replaced at ... intervals. Due to the induced radioactivity this will have to be done remotely, using robotic technology. Although this technology is widely available in the nuclear industry this whole beam dump is a large and costly affair for the ILC and any future HEP accelerators.

An alternative approach utilizes the huge acceleration gradients from PWFA. This idea was proposed in 2010 by Wu et al. [4]. They showed through simulations that a 500 MeV electron bunch, under certain conditions, could lose up to 70% of its energy by propagating a few millimetres through a dense plasma, a so-called passive plasma beam dump. Full energy depletion was prevented by decelerated particles in the bunch reaching non-relativistic speeds and falling behind the main bunch, at which point they were picked up by the accelerating portion of the field and reaccelerated to relativistic speeds, the bunch energy is said to have saturated. It was further found that the decelerating field was independent of the initial bunch energy, such that the distance to saturation scaled linearly with bunch energy, such that a 100 GeV bunch would require 20 cm to lose 70% of its energy. To avoid re-acceleration they strategically placed thin aerogel foils in the plasma to stop the low energy particles before re-acceleration. Using this improved the energy depletion up to 90% for 500 MeV bunch. Due to the finite response time of the plasma, the head of the bunch displaces the plasma electrons and sets up the wakefield but due not experience the huge decelerating gradients further back. For this reason the head of the bunch loses essentially no energy, known as "energy chirp", as can be seen in the original plots from the paper by Wu et al. in figure 1.1. For a 500 MeV or a few GeV bunch this might not be a major issue since smaller conventional beam dumps could be used to dump this remaining energy. For energies of 100s of GeV however this energy chirp could still pose an issue in terms of radioactivity of materials. Furthermore, it is not clear how the proposed intermediate foils would degrade and behave under the extreme conditions of high-energy beams.

To address the energy chirp Bonatto et. al [5] proposed the so-called active beam dump, whereby a laser is driven through the plasma in front of the bunch that is to be decelerated. By carefully positioning the laser in relation to a 1 GeV bunch it was shown that the energy

in the head of the bunch could be significantly reduced, resulting in a total energy depletion up to 95%. It is however difficult to apply this method to higher energy bunches since the dispersion of the laser in the plasma prevents laser propagation over long distances.

Finally, Hanahoe et al. [6] proposed the use of varying plasma density instead of foils as an alternative way to prevent reacceleration. Linear or quadratically increasing plasma densities were shown to achieve comparable reduction of the reaccelerated particles as the foils used by Wu et al. It is however unclear whether such plasma density profiles can be set up and sustained reliably in an experimental setting.

With several proposed plasma beam dump techniques in place this project endeavours to merge the passive and active approaches in what we call a hybrid plasma beam dump, with the goal of achieving a full energy depletion of the bunch. In addition, simulations will also be carried out for a recently approved plasma beam dump experiment at the FLASHForward facility at DESY in Germany. This will be the first dedicated plasma beam dump experiment of its kind and will be capable of testing both the passive and active approaches described above.

1.4 Outline of report

This intermediate report details the initial phase of a full-year project on plasma wakefield deceleration and is written in partial fulfilment of the requirements for the degree of Master in Physics. As such, it does not attempt to cover the full scope of the work and research conducted in the first half of this project, but rather aims to provide an introduction to the field, establish the theoretical background and construct the computational framework necessary to perform the intended research. Having laid the groundwork for the project in this report, the final-year report will reap the rewards of this work by presenting the full results and outcome of the project.

The theory behind plasma wakefield acceleration and plasma beam dumps is covered in section 2. The simulation framework is detailed in section 3, followed by simulation tests and preliminary results in section 4. We conclude this report by summarising the work that has been presented and looking ahead at the work that is to be carried out in the second half of this project.

Superconduction RF (<https://www.youtube.com/watch?v=HqrSb36QYVk>)

2

Theoretical foundations

2.1 Introduction

In this chapter we introduce the linear fluid model of plasma wakefield acceleration and derive the equations governing the response of a plasma to an electron bunch propagating through. This model assumes that the bunch is ultra-relativistic and that the plasma density is much higher than the bunch density, which will allow us to treat the plasma response as a first order perturbation to the background density. We also discuss the non-linear, so-called "blowout", regime which can not be treated perturbatively and is characterised by the expulsion of plasma electrons in a volume behind the bunch. The response to a laser being driven through the plasma, the so-called ponderomotive force response, shares many similar features to the theory presented in this chapter but presents other issues such as dissipation and de-phasing in the plasma which will need to be addressed in the context of the active beam dump. For this reason the theory of laser-plasma interactions will be covered in a subsequent report.

2.2 Linear fluid model

In this section, we derive the response of a plasma to an electron bunch by considering the plasma electrons as a fluid. We shall make the assumptions; (i) the initial plasma is uniform and electrically neutral everywhere; (ii) the plasma ions can be considered stationary since for all plasmas the mass of the ions is much larger than the electron mass, $m_{\text{ion}} \gg m_e$; (iii) the electron bunch is ultra-relativistic, $v/c \approx 1$, such that the density distribution of the bunch does not evolve as it interacts with the plasma; (iv) the bunch density is much less than the plasma electron density, $n_b \ll n_p$. A beam propagating through a plasma satisfying these conditions is said to be in the *linear regime*. The dynamics of the plasma electrons is governed by the continuity equation

$$\frac{\partial n_p}{\partial t} = -\nabla \cdot (n_p \mathbf{v}_p) \quad (2.1)$$

where n_p is the plasma electron density density and \mathbf{v}_p the plasma fluid velocity. This simply ensures charge conservation by imposing that the plasma electron density change in a given volume is due to plasma electrons flowing in or out. The evolution of the electromagnetic

fields in the plasma is governed by Maxwell's laws:

$$\nabla \cdot \mathbf{E} = 4\pi\rho \quad (2.2)$$

$$\nabla \cdot \mathbf{B} = 0 \quad (2.3)$$

$$\nabla \times \mathbf{E} = -\frac{1}{c} \frac{\partial \mathbf{B}}{\partial t} \quad (2.4)$$

$$\nabla \times \mathbf{B} = \frac{4\pi}{c} \mathbf{J} + \frac{1}{c} \frac{\partial \mathbf{B}}{\partial t} \quad (2.5)$$

which in turn determine the response of the plasma fluid through the Lorentz force law:

$$m_e \frac{\partial n_p \mathbf{v}_p}{\partial t} = e n_p \left(\mathbf{E} + \frac{\mathbf{v}_p \times \mathbf{B}}{c} \right). \quad (2.6)$$

We now make use of assumption (iv) which allows us to treat the plasma response to a particle beam perturbatively such that $n_p = n_0 + n_1$, where n_0 is the unperturbed uniform electron density and $n_1 \ll n_0$ is the perturbation from interacting with the electron bunch. This perturbation also requires that the change in fluid velocity upon interacting with the bunch is small, such that $v_p \ll c$. Substitution into the continuity equation yields

$$\frac{\partial n_1}{\partial t} = -n_0 \left(1 - \frac{n_1}{n_0} \right) \nabla \cdot \mathbf{v}_p \quad (2.7)$$

Taking the time differential and neglecting terms $\mathcal{O}(n_1/n_0)$ then gives

$$\frac{\partial^2 n_1}{\partial t^2} = -n_0 \frac{\partial(\nabla \cdot \mathbf{v})}{\partial t} \quad (2.8)$$

Similarly, substitution into the Lorentz force law gives to first-order

$$m_e \frac{\partial \mathbf{v}}{\partial t} = e \mathbf{E} \quad (2.9)$$

which, using Gauss's law, gives

$$\frac{\partial(\nabla \cdot \mathbf{v})}{\partial t} = \frac{e^2}{m_e} 4\pi(n_1 + n_b) \quad (2.10)$$

where n_b is the charge density of the electron bunch. Equations (2.8) and (2.10) hence give

$$\frac{\partial^2 n_1}{\partial t^2} + \omega_p^2 n_1 = -\omega_p^2 n_b \quad (2.11)$$

where

$$\omega_p = \sqrt{\frac{4\pi e^2 n_0}{m_e}} \quad (2.12)$$

is the plasma frequency. Hence the plasma density perturbation is described by a second-order differential equation with the bunch acting as a source term. We proceed to solve this for a radially symmetric bunch by evaluating equation (2.11) in a reference frame co-moving with the electron bunch, where the coordinate $\xi = x - ct$ represents the position along the bunch as it travels in the x -direction. Doing this yields

$$-\frac{1}{k_p^2} \left(\frac{\partial^2}{\partial \xi^2} + k_p^2 \right) n_1(r, \xi) = n_b(r, \xi) \quad (2.13)$$

where $k_p = \omega_p/c$ is the wavenumber and causality demands that $n_1(r, \xi < 0) = 0$. We evaluate this by finding the Green's function $G(\xi, \xi')$, which by definition obeys

$$-\frac{1}{k_p^2} \left(\frac{\partial^2}{\partial \xi^2} + k_p^2 \right) G(\xi, \xi') = \delta(\xi - \xi') \quad (2.14)$$

which gives

$$G(\xi, \xi') = \begin{cases} 0 & , -\infty < \xi < \xi' \\ A(\xi') \sin(k_p \xi) + B(\xi') \cos(k_p \xi) & , \xi' < \xi < \infty \end{cases} \quad (2.15)$$

where the constant $A(\xi')$ and $B(\xi')$ are determined by requiring continuity at $\xi = \xi'$ and by integrating equation (2.14) across this same boundary. This yields

$$G(\xi, \xi') = k_p \Theta(\xi - \xi') (\cos(k_p \xi) \sin(k_p \xi') - \cos(k_p \xi') \sin(k_p \xi)) \quad (2.16)$$

and the resulting plasma perturbation is

$$\begin{aligned} n_1(r, \xi) &= \int_{-\infty}^{\infty} G(\xi, \xi') n_b(r, \xi') d\xi' \\ &= \int_{-\infty}^{\xi} \sin(k_p(\xi - \xi')) n_b(r, \xi') d\xi' \end{aligned} \quad (2.17)$$

where we have used the trigonometric identity for $\sin(k_p(\xi - \xi'))$. Hence the electron bunch induces oscillatory density perturbations in the plasma with a wavelength given by $\lambda_p = 2\pi/k_p$. In addition, the magnitude of these perturbation scales linearly with n_b , the density of the beam driver. Equation (2.12) further shows that these perturbations scale as $n_0^{1/2}$, the square root of the plasma density. These perturbations set up electromagnetic fields in the plasma behind the beam driver. An understanding of these fields is crucial in order to design a functioning plasma wakefield experiment.

2.2.1 Longitudinal Accelerating Field

The electric field parallel to the propagation of the beam driver is what drives particles to either accelerate or decelerate. This is called the longitudinal plasma wakefield and in this section we proceed to derive an expression for it in the linear regime considered above. From Maxwell's equations (2.2-2.5) it is straightforward to show that the electric field in the plasma obeys a wave equation:

$$\nabla^2 \mathbf{E} - \frac{1}{c^2} \frac{\partial^2 \mathbf{E}}{\partial t^2} = \frac{4\pi}{c^2} \frac{\partial \mathbf{J}}{\partial t} + 4\pi \nabla \rho \quad (2.18)$$

where the change in current and variations in the charge density act as source terms. Letting $\rho = \rho_b + \rho_p$ be the total charge density and $\mathbf{J} = \mathbf{J}_b + \mathbf{J}_p$ be the total charge current, where b and p denote the beam and plasma respectively, we have from equation (2.9) that

$$\frac{\partial \mathbf{J}_p}{\partial t} = \frac{e^2 n}{m} \mathbf{E} \quad (2.19)$$

Substituting this into equation (??), together with $\mathbf{J}_b = c\rho_b\hat{\mathbf{z}}$, and taking the z-component gives

$$\left(\nabla^2 - \frac{1}{c^2} \frac{\partial^2}{\partial t^2} - k_p^2\right) E_z = \frac{4\pi}{c} \frac{\partial \rho_b}{\partial t} + 4\pi \frac{\partial}{\partial z} (\rho_b + \rho_p) \quad (2.20)$$

where $k_p = \omega_p/c$ is the plasma wave number and E_z is the longitudinal electrical field. To solve this we write $\nabla^2 = \nabla_\perp^2 + \partial_z^2$ in transverse and longitudinal components. Furthermore, we proceed to work in Fourier transform space, where

$$E_z(\xi) = \frac{1}{2\pi} \int_{-\infty}^{\infty} \tilde{E}_z(k) e^{ik\xi} dk \quad (2.21)$$

and similarly for ρ_b and ρ_p . Equation (2.20) now simplifies to

$$\left(\nabla_\perp^2 - k_p^2\right) \tilde{E}_z(\xi) = 4\pi i k \tilde{\rho}_p \quad (2.22)$$

We note that the two contributions from the beam cancel each other out, this is because of relativistic effects (?) [?]. The effect of the beam is however represented in the plasma modulations. Write equation () in Fourier transform space gives

$$\tilde{\rho}_p = \frac{k_p^2}{k^2 - k_p^2} \tilde{\rho}_b \quad (2.23)$$

which together with the cylindrical representation of the Laplacian

$$\nabla_\perp^2 = \frac{1}{r} \frac{\partial}{\partial r} r \frac{\partial}{\partial r} + \frac{1}{r^2} \frac{\partial^2}{\partial \phi^2} \quad (2.24)$$

gives

$$\left(\frac{\partial^2}{\partial r^2} + \frac{1}{r} \frac{\partial}{\partial r} - k_p^2\right) \tilde{E}_z = 4\pi i k_p^2 \frac{k}{k^2 - k_p^2} \tilde{\rho}_b \quad (2.25)$$

We now rewrite this equation as

$$\mathcal{L}\tilde{E}_z = \tilde{f}(r) \quad (2.26)$$

We proceed as before and solve this PDE by finding the Green's function. Working in a cylindrical coordinate system we have that the Green's function must satisfy

$$\mathcal{L}G(\mathbf{r}, \mathbf{r}') = \delta(\mathbf{r} - \mathbf{r}') = \frac{1}{r} \delta(r - r') \delta(\phi - \phi') \delta(z - z') \quad (2.27)$$

where the RHS is the 3D Dirac delta function in cylindrical polar coordinates, defined such that $\int \delta(\mathbf{r} - \mathbf{r}') r dr d\phi dz = 1$. Letting

$$G(\mathbf{r}, \mathbf{r}') = G_r(r, r') \delta(\phi - \phi') \delta(z - z') \quad (2.28)$$

leads to

$$\mathcal{L}G_r(r, r') = \frac{1}{r} \delta(r - r') \quad (2.29)$$

The LHS of this expression is the modified Bessel function of order zero and the RHS represents our source term. Consequently the Green's function is formed by linear combinations of the linearly independent, modified Bessels functions of order zero.

$$G(r, r') = \begin{cases} A(r')(A_1 I_0(k_p r) + B_1 K_0(k_p r)) & , 0 < r < r' \\ B(r')(A_2 I_0(k_p r) + B_2 K_0(k_p r)) & , r' < r < \infty \end{cases} \quad (2.30)$$

requiring that the two parts of this expression each satisfy one of the B.Cs we have that $B_1 = A_2 = 0$ since $K_0(k_p r) \rightarrow \infty$ as $r \rightarrow 0$ and $I_0(k_p r) \rightarrow \infty$ as $r \rightarrow \infty$. Continuity in $G(r, r')$ at $r = r'$ further gives that

$$G(r, r') = A_0 \begin{cases} I_0(k_p r) K_0(k_p r') & , 0 < r < r' \\ I_0(k_p r') K_0(k_p r) & , r' < r < \infty \end{cases} \quad (2.31)$$

where A_0 is a constant of proportionality that we find by integrating $\mathcal{L}G(r, r') = \delta(r - r')/r$ with respect to r across the interval $[r' - \epsilon, r' + \epsilon]$, which needs to be satisfied for all ϵ , including the limit as $\epsilon \rightarrow 0$.

$$\lim_{\epsilon \rightarrow 0} \int_{r' - \epsilon}^{r' + \epsilon} \left(\frac{\partial^2 G}{\partial r^2} + \frac{1}{r} \frac{\partial G}{\partial r} - k_p^2 G \right) dr = \lim_{\epsilon \rightarrow 0} \int_{r' - \epsilon}^{r' + \epsilon} \frac{1}{r} \delta(r - r') dr = \frac{1}{r'} \quad (2.32)$$

$$\lim_{\epsilon \rightarrow 0} \left[\frac{1}{k_p} \frac{\partial G}{\partial r} \right]_{z-\epsilon}^{z+\epsilon} = \frac{A_0}{k_p} \left(I_0(k_p r') \frac{\partial K_0(k_p r)}{\partial r} - \frac{\partial I_0(k_p r)}{\partial r} K_0(k_p r') \right) \Big|_{r=r'} = \frac{1}{r'} \quad (2.33)$$

This equality must hold for all values of r' . Hence, following an approach by Jackson [7], we evaluate the LHS for $r' \gg 1$, where I_0 and K_0 take the limiting forms

$$I_0(k_p r') \rightarrow \frac{1}{\sqrt{2\pi k_p r'}} e^{k_p r'} \quad \text{and} \quad K_0(k_p r') \rightarrow \sqrt{\frac{\pi}{2k_p r'}} e^{-k_p r'} \quad (2.34)$$

which implies that $A_0 = -1$.

$$G(r, r') = -I_0(k_p r) K_0(k_p r') \Theta(r' - r) - I_0(k_p r') K_0(k_p r) \Theta(r - r') \quad (2.35)$$

We can thus find \tilde{E}_z from

$$\tilde{E}_z(r, k) = \int_{-\infty}^{\infty} G(r, r') f(r', k) r' dr' \quad (2.36)$$

and then perform an inverse Fourier transform to find

$$E_z(r, \xi) = \frac{1}{2\pi} \int_{-\infty}^{\infty} \tilde{E}_z(r, k) e^{ik\xi} dk \quad (2.37)$$

Doing this yields

$$E_z(r, \xi) = -2ik_p^2 \int_{-\infty}^{\infty} \frac{ke^{ik\xi}}{k^2 - k_p^2} dk \int_0^{\infty} (I_0(k_p r) K_0(k_p r') \Theta(r' - r) + I_0(k_p r') K_0(k_p r) \Theta(r - r')) \tilde{\rho}_b(r') r' dr' \quad (2.38)$$

For a known beam distribution $\rho_{b0}(r, \xi)$ (add ξ in all previous expressions?) this expression can be used to compute the resulting longitudinal electric field. We shall now proceed by calculating this for a bi-Gaussian bunch distribution. To do this, we could compute the electric field from the Green's function directly and then carrying out the inverse Fourier transform, or we could choose to first compute the field due to a point-particle and then convolving it with the bi-Gaussian distribution. We proceed by doing the latter by following the approach of Dawson [8] ; we choose a charge distribution with radial symmetry and a delta function in the z -direction to match our Green's function.

$$\rho_{b0}(r, \xi) = \frac{e}{2\pi r} \delta(r - r_0) \delta(\xi) \Rightarrow \tilde{\rho}_{b0}(r, k) = \int_{-\infty}^{\infty} \rho_{b0}(r, \xi) e^{-ik\xi} d\xi = \frac{e}{2\pi r} \delta(r - r_0) \quad (2.39)$$

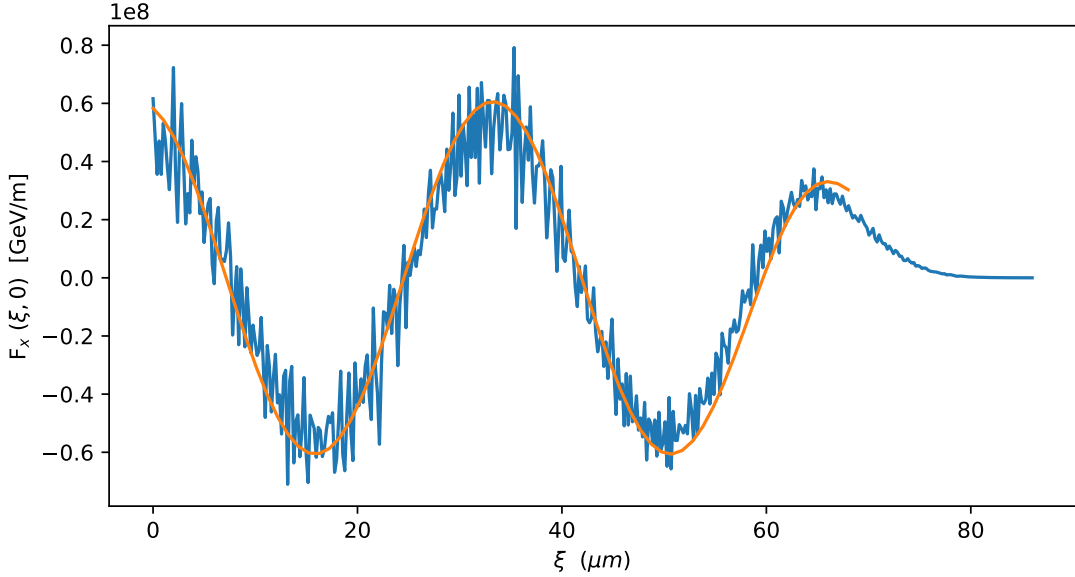


Figure 2.1: Simulation vs. theory for linear regime with $n_p/n_b = 100$.

Substituting this into equation (2.38) and performing a contour integrating in k-space yields

$$E_z(r, \xi) = -2ek_p^2 \cos(k_p \xi) G(r, r_0) \Theta(\xi), \quad (2.40)$$

where $\Theta(\xi)$ ensures causality is preserved. This is the so called single-particle wake function [Dawson]. The longitudinal electric field resulting from an arbitrary radially-symmetric source distribution $n_b(r, \xi)$ is now given by convolving the source by the single-particle wake function:

$$E_z(r, \xi) = -2ek_p^2 \int_0^{2\pi} d\phi \int_{-\infty}^{\infty} \cos(k_p(\xi - \xi')) \Theta(\xi - \xi') d\xi' \int_0^{\infty} G(r, r_0) n_b(r_0, \xi') r' dr' \quad (2.41)$$

$$= -4\pi e k_p^2 \int_{-\infty}^{\xi} \cos(k_p(\xi - \xi')) d\xi' \int_0^{\infty} G(r, r_0) n_b(r_0, \xi') r_0 dr_0 \quad (2.42)$$

The electric force is thus $F_z(r, \xi) = -eE_z(r, \xi)$. To compare with simulations and experiments we now choose to convert from CGS to SI units by having $e^{\text{CGS}} \rightarrow e^{\text{SI}}/\sqrt{4\pi\epsilon_0}$. The electric force in SI units (J/m) is thus

$$F_z(r, \xi) = \frac{e^2 k_p^2}{\epsilon_0} \int_{-\infty}^{\xi} \cos(k_p(\xi - \xi')) d\xi' \int_0^{\infty} G(r, r_0) n_b(r_0, \xi') r_0 dr_0 \quad (2.43)$$

This expression can be calculated numerically to ; fig. ??

2.2.2 Transverse Focusing Field

An ultrarelativistic electron bunch will be highly contracted in the direction of propagation relative to the plasma electrons in the 'lab' frame. Assuming $\beta = 1$ as before the electric field due to the bunch is purely radial, E_r . In addition, the magnetic field due to the

charge is azimuthal, B_θ . The resulting transverse wakefield $W_\perp = E_r - B_\theta$ experienced by a realtivisit particle due to the wake is given by the *Panofsky-Wenzel theorem*[9], which says that the transverse wakefield at a position ξ behind the head of the bunch is related to the longtiduinal wakefield W_\parallel via

$$\frac{\partial W_\perp}{\partial \xi} = \frac{\partial W_\parallel}{\partial r} . \quad (2.44)$$

Since $W_\parallel = E_z$ this gives a transverse wakefield

$$W_\perp(\xi) = \int \frac{\partial E_z}{\partial r} d\xi . \quad (2.45)$$

The transverse force on a bi-Gaussian bunch can now by found by applying this expression to on the longitudinal single-particle wakefield (2.40) and then performing the same convolution as above, which yields

$$F_r(r, \xi) = \frac{e^2 k_p^2}{\epsilon_0} \int_{-\infty}^{\xi} \sin(k_p(\xi - \xi')) d\xi' \int_0^\infty \frac{1}{k_p} \frac{\partial G(r, r_0)}{\partial r} n_b(r_0, \xi') r_0 dr_0 \quad (2.46)$$

2.3 Non-linear Regime

What is the self-injection threshold

2.3.1 Wave-breaking field

Dawson's derivation [Note: The wave-breaking field does not represent the onset of the non-linear regime but the highest achievable field in the non-linear regime.] We consider a simple 1D linear non-relativistic electron sheet model first used by Dawson [10] to show the breakdown of the linear model (**correct?**). Consider the plasma being made up of thin sheets of ions and electrons. A sheet at equilibrium position $z = z_0$ is then displaced by $\eta_0(z_0)$, where the displacement is set as function of the equilibrium position for full generality, to a new position $z = z_0 + \eta_0$. The displaced sheet reveals a positive surface charge density $\sigma = en_0\eta_0$, where n_0 is the electron charge density in the plasma. This sets up a restoring electric field which we find using Gauss's law to be $E_{\text{res}} = 4\pi n_0 e \eta_0$ which yields a restoring force

$$m_e \frac{\partial^2 \eta_0}{\partial t^2} = -e E_{\text{res}} = -4\pi n_0 e^2 \eta_0 = -\omega_p^2 \eta_0 \quad (2.47)$$

with solutions

$$\eta_0(z_0, t) = A_1(z_0) \cos(\omega_p t) + A_2(z_0) \sin(\omega_p t) \quad (2.48)$$

The phenomena of wave breaking can be shown by considering another electron sheet at an equilibrium position $z_1 = z_0 + \Delta z_0$ at a distance Δz_0 away from the first sheet. This sheet is then displaced by η_1 to a new position $z_1^* = z_0 + \Delta z_0 + \eta_1$. The linear model is valid provided that there are no electron trajectories intersect one another in the plasma [**is this correct? Why does the model break down?**]. Hence the model is valid provided that $z_1^* - z_0 > z - z_0$ which implies that we must have

$$\Delta z_0 + \eta_1 > \eta_0 , \quad (2.49)$$

for all $\Delta z_0 \in \mathbb{R}$, to sustain plasma oscillations in the linear model. We now consider the limit as $\Delta z_0 \rightarrow 0$ for the expression

$$\frac{\partial \eta}{\partial x_0} = \lim_{\Delta z_0 \rightarrow 0} \frac{\Delta \eta}{\Delta z_0} = \lim_{\Delta z_0 \rightarrow 0} \left(\frac{\eta_1 - \eta_0}{\Delta z_0} \right) > \lim_{\Delta z_0 \rightarrow 0} \left(\frac{\eta_0 - \Delta z_0 - \eta_0}{\Delta z_0} \right) = -1 \quad (2.50)$$

which simplifies to

$$\frac{\partial \eta}{\partial z_0} > -1 \quad (2.51)$$

where the inequality is introduced using Eq. (2.49). We now consider the special case where $A_1(z_0) = A \sin(k_p z_0)$ and $A_2(z_0) = 0$. This is a valid solution since $\sin(k_p z_0)$ is single-valued for all $k_p, x_0 \in \mathbb{R}$. This particular solution is chosen to highlight the breakdown of the electric field, and is motivated by (**[what?]**) the solution we found for the electric field in section 2. Applying the no-crossing criterion in Eq. 2.51 to $\eta = \eta_0(z_0, t)$ yields

$$\frac{\partial \eta_0}{\partial z_0} = Ak_p \cos(k_p z_0) > -1 \Leftrightarrow Ak_p \leq 1 \quad (2.52)$$

which gives the maximum amplitude as $A_{max} = 1/k_p$. Hence the maximum restoring electric field $E_{max} \equiv E_{wb} = 4\pi n_0/k_p$ is given by

$$E_{wb} = \frac{m_e v_p \omega_p}{e} \quad (2.53)$$

the so-called *wave-breaking field*. To further show how this breaks the linear model we consider the effect on the electric field up to and past the wave-breaking limit. As above we have,

$$z = z_0 + \eta_0 = z_0 + A \sin(k_p z_0) \quad (2.54)$$

and

$$E = 4\pi n_0 e A \sin(k_p z_0) \quad (2.55)$$

from which we want to find the electric field as a function of z . We can do this by numerically solving Eq. 2.54 for z_0 in a range of z values given fixed values of A . This gives $z_0 = z_0(z, A)$ which can be substituted into Eq. 2.55 to give $E = E(z, A)$, the result of which is shown in Fig. 2.2. From this we conclude that the electric field is no longer single-valued for $A > 1/k_p$, i.e past the electric field's wave-breaking amplitude, which signifies a breakdown of the linear model.

This is further emphasized by consider the electron-density response as $\partial\eta/\partial z_0 \rightarrow -1$. To do this we use Eq. XXX in 1D with no beam density $n_b = 0$,

$$\frac{\partial E}{\partial z} = 4\pi e(n_0 - n) \quad (2.56)$$

where $n = n_0 + n_1$ is the perturbed plasma density and n_0 is the ion density, hence $n_0 - n$ is the free (negative) charge density in the plasma. We now take the derivative of the perturbed electric field and substitute the above expression

$$\frac{\partial E}{\partial z} = 4\pi n_0 e \frac{\partial \eta}{\partial z} \Rightarrow n = n_0 \left(1 - \frac{\partial \eta}{\partial z}\right) \quad (2.57)$$

We now rewrite $\partial/\partial z$, using $z = z_0 + \eta$, as

$$\frac{\partial}{\partial z} = \left(1 - \frac{\partial \eta}{\partial z_0}\right)^{-1} \frac{\partial}{\partial z_0} \quad (2.58)$$

which gives

$$n = \frac{n_0}{1 + \frac{\partial \eta}{\partial z_0}} \quad (2.59)$$

which means that the perturbed electron density grows infinite as $\partial\eta/\partial z_0 \rightarrow -1$, again signifying the breakdown of the linear model.

Having seen that the linear theory can break down mathematically, it is crucial to ask whether this is realised in 3D models and experiments as well.

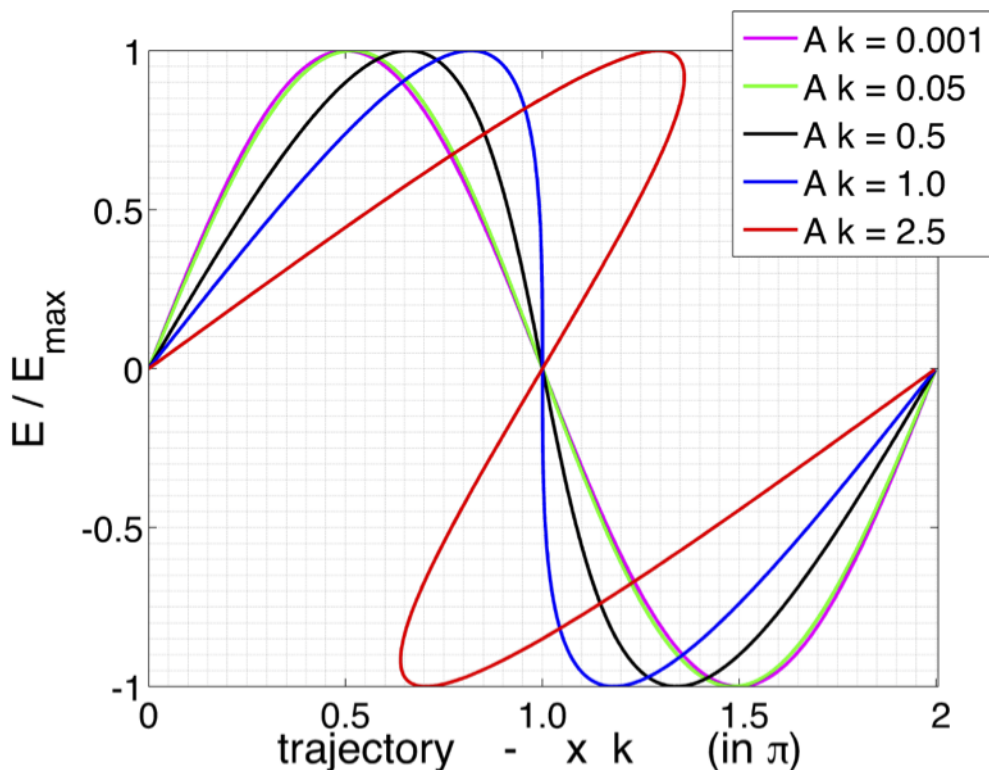


Figure 2.2: Plot corresponding to Dawson's derivation of the wave-breaking field [ref. Sahai].

2.4 Particle interactions with matter

Conventional beam dumps work by stochastic interactions of the beam with the dense medium [hanahoe 6.5]

2.4.1 Bohr-Fermi-Bethe-Bloch Theory

Bethe-Bloch formula:

$$-\left\langle \frac{dU}{ds} \right\rangle_{\text{ion}} = \frac{4\pi e^4 n_{e,m}}{m_e c^2 \beta^2} \left[\ln \left(\frac{2m_e \gamma^2 v^2}{I} \right) - \beta^2 \right] \quad (2.60)$$

2.4.2 Collective Plasma Deceleration – Non-Linear regime

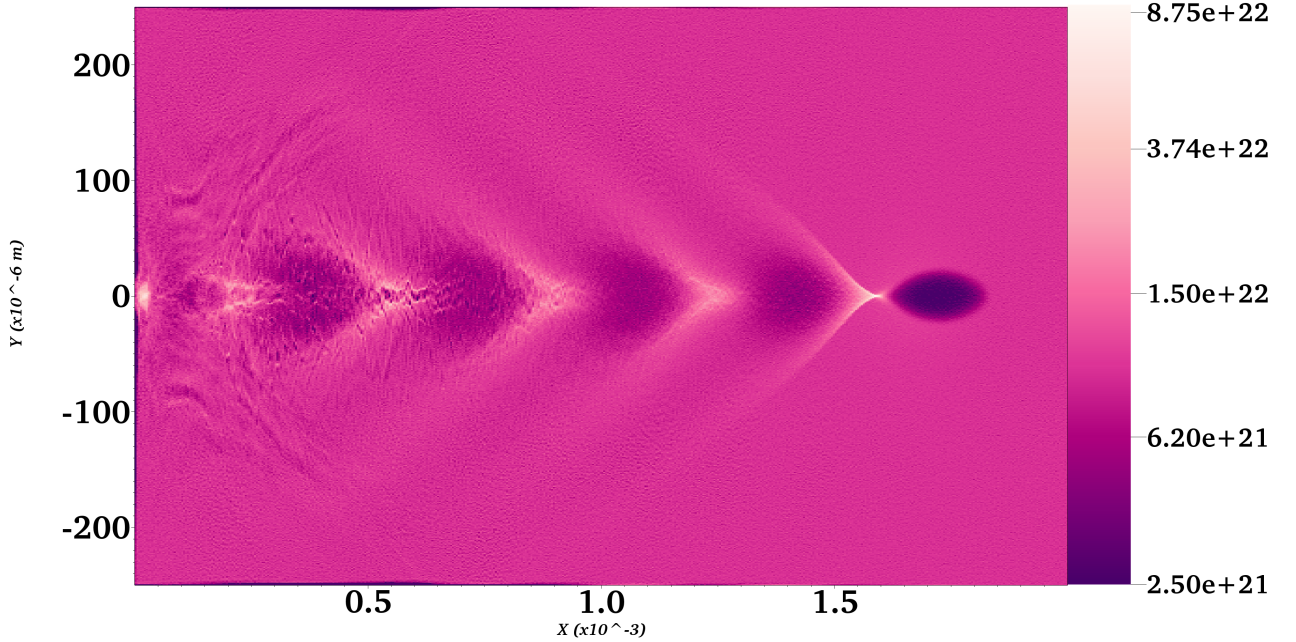


Figure 2.3: Non-linear regime, plasma density perturbations. Added custom legend with density=number of electrons / grid-square size.

$$-\left(\frac{dE}{dz}\right)_{\text{coll-wave-break}} = F_e = eE_{\text{wave-break}} = m_e c \omega_p \left(\frac{n_b}{n_e}\right) \quad (2.61)$$

What is the wave-breaking electric field?

2.4.3 Collective Plasma Deceleration – Linear regime

Based on the work of Lu et. al [11], wherein it was shown that the predictions from the linear models perform well even in the non-linear regime, it is of interest to compute the energy loss in the linear regime. This follows the analysis by Bonatto et al. [12].

The energy loss of a bunch is due to the work carried out by the longitudinal electric field E_z , neglecting effects such as bremsstrahlung etc. The rate of energy change with propagation distance of a particle at position (r, ξ) in the bunch after travelling is given by the force exerted on the particle by the longitudinal electric field:

$$\frac{dU_p}{ds} = -eE_z(r, \xi) \quad (2.62)$$

where we have assumed that there occurs no modulation of the particle bunch as it traverses the plasma, hence the electric field is only a function of the position in the bunch $E_z(r, \xi)$ and not the propagation distance s . Integrating over the propagation distance then gives

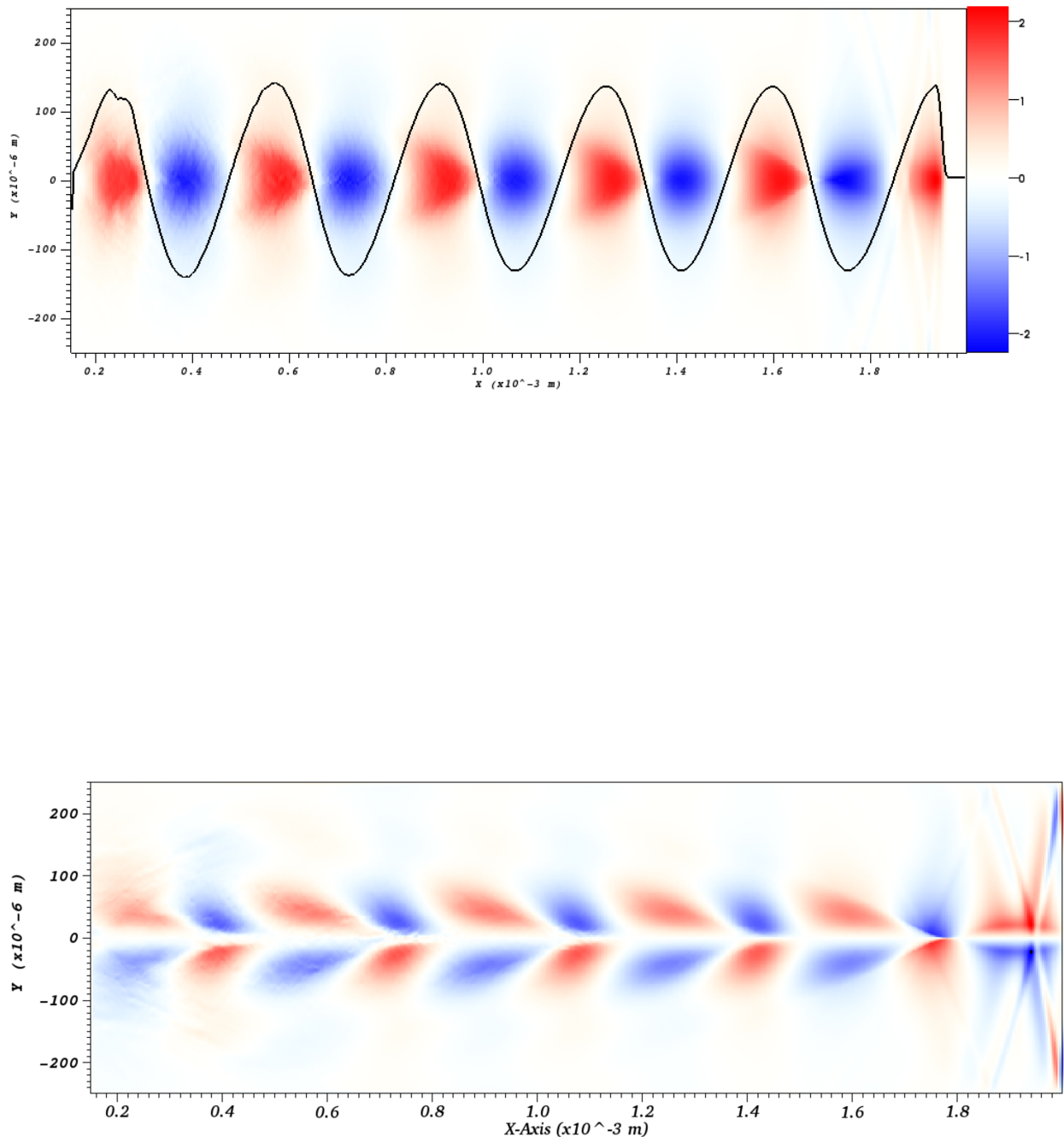


Figure 2.4: Should these three plots be in results or here? OR PUT SIMUALTIONS CHAPTER BEFORE THEORY CHAPTER. Then theory can be used to also verify that simulations work. Probably not, better explain everything to motivate what simulations to be done

the energy of one particle in the beam at position (r, ξ) after travelling a distance s :

$$U_e(r, \xi, s) = U_e(r, \xi, 0) - seE_z(r, \xi) \quad (2.63)$$

from which multiplication by the beam number density $n_b(r, \xi)$ and integration over the volume of the bunch gives the total energy of all particles in the bunch after propagation distance s

$$U(s) = \int U_e(r, \xi, 0) n_b(r, \xi) r dr d\xi d\phi - se \int E_z(r, \xi) n_b(r, \xi) r dr d\xi d\phi \quad (2.64)$$

where $dV = r dr d\xi d\phi$ [I think].

2.4.4 Notes Bonatto

Rate of change due to the longitudinal electric field acting on an electron beam, i.e position beam in the decelerating region of the wakefield.

"the beam only experiences its self-excited wakefield."

In the passive beam dump, are we essentially slowing down a "drive bunch" without having a witness bunch behind to get accelerated?

It is probably better to use gamma as in Bonatto's paper, to make it easier to explain total beam energy integral. Basically integrate over all particles.

$$U = \gamma m_e c^2 - \frac{dU}{ds} = (F_e)_z = eE_z \quad (2.65)$$

where s is the distance travelled in the plasma and U is the energy of a particle in the beam at position ξ . for ultra relativistic beams, $\beta \sim 1$, the longitudinal electric field is a function of the position along the bunch $\xi = z - ct$ and not z explicitly.

$$U(s, \xi) = U_0 - esE_z(\xi) \quad (2.66)$$

The total energy of the beam after travelling a distance s is then found by integrating across all the particles in the beam, which is integrating across ξ since analysis is in 1-D.

$$\mathcal{U}(s) = U_0 \int_{-\infty}^{\infty} \quad (2.67)$$

We will proceed by calculating the gamma factor of a given particle in the beam who's energy we wish to compute.

$$\gamma(s, \xi) = \gamma_0 - esE_z(\xi) \quad (2.68)$$

Aanja

3

Simulations

- Ways to simulate plasmas, different techniques/codes etc.

3.1 Plasma simulations

Why simulations

Simulations because: Cheaper than experiments, more readily available to anyone, simulations allow us to study, understand and exploit these phenomena without the need to repeatedly perform expensive and intricate experiments...Furthermore, by having a simulated rather than physical experiment, one may avoid the uncertainties and noise present in the real world and may therefore investigate and even discover physical phenomena that are too sensitive to be detected in noisy data samples. To take advantage of simulations it is however crucial to know the accuracy by which the simulations model the physical situation and to understand the limitations that this imposes. For instance, as will be shown in section XXX, failing to model the experiment with high enough resolution can lead to phenomena emerging from purely numerical features in the simulations. One must therefore be confident that the results seen in simulations accurately represent the physics at hand, either by comparing the simulations to experimental data or theoretical calculations if available. The non-linear nature of the high-energy plasma wakefield phenomena that we wish to model in this project do not lend themselves easily to analytical treatments. To investigate these phenomena and provide useful results for future experiments we will make extensive use of simulations in this project.

Given that a plasma is no more than electrons and ions interacting electromagnetically, the response of such a plasma to the propagation of an electron bunch or laser pulse could in theory be simulated by solving Maxwell's equations for a set of initial conditions. This would involve solving Maxwell's equations at time an initial time t_0 and calculating the combined electromagnetic fields acting on each particle in the plasma. Then, by considering each particles velocity, one could calculate the new positions and velocities of all particles for a small time increase $t_0 + \Delta t$. Repeating these computation would lead us to find the approximate plasma response at any arbitrary time $t > t_0$. However, this approach is computationally intractable. Since if we attempt this approach in most plasma simulations. For instance, if we consider that the plasma in a typical plasma wakefield accelerator [Hanahoe] is on the order of centimetres in extent, with a number density $10^{20} m^{-3}$, we find that we have on the order of 10^{14} electrons in the plasma. All these electrons would have to be included in the simulation and stored with their associated 6-dimensional position and velocity data (x, y, z, v_x, v_y, v_z) . Each number would be stored as a 32-bit double precision floating point number, yielding the total data size required for the whole plasma simulation on the order

of a petabyte (10^{15} bytes).

To circumvent this computational road block we make use of so-called Particle-In-Cell (PIC) codes, in which a large collections of physical microscopic particles are represented as smaller collections of macroscopic pseudo-particles on a grid. In this chapter we outline the general PIC approach and introduce the plasma physics PIC code EPOCH, which is used throughout this project. We further detail the modifications necessary to allow the hybrid beam dump scheme to be simulated on EPOCH.

3.2 Particle-in-Cell Codes

Starting from EM fields $\mathbf{E}_{(n)}$, $\mathbf{B}_{(n)}$ and charge current $\mathbf{J}_{(n)}$ present at iteration n [at a specific position, middle of Yee grid?] we obtained the fields at the next time step $n+1$ by computing the resulting fields and currents at an intermediate half-way step $n + 1/2$. We do this by first computing the change in the electric field, using Ampere's law, $\Delta\mathbf{E}_{(n)}$ which we add to our current field such that

$$\mathbf{E}_{(n+1/2)} = \mathbf{E}_{(n)} + \frac{\Delta t}{2} \left(c^2 \nabla \times \mathbf{B}_{(n)} - \frac{\mathbf{J}_{(n)}}{\epsilon_0} \right) \quad (3.1)$$

from this the magnetic field is given by

$$\mathbf{B}_{(n+1/2)} = \mathbf{B}_{(n)} - \frac{\Delta t}{2} \left(c^2 \nabla \times \mathbf{E}_{(n+1/2)} \right) \quad (3.2)$$

(at which point the particle pusher, detailed below, updates the current to $\mathbf{J}_{(n+1)}$)
at which point we need to update the current to $\mathbf{J}_{(n+1)}$ in order to proceed finding the fields at time step $n + 1$. This is done using the particle pusher. We update the position of each particle

$$\mathbf{x}_{(n+1/2)} = \mathbf{x}_{(n)} + \frac{\Delta t}{2} \mathbf{v}_{(n)} \quad (3.3)$$

from which we also obtain the intermediate velocity $\mathbf{v}_{(n)}$ [correct?]. Using the Lorentz force law we then compute the force $\mathbf{F}_{(n)} = \Delta p / \Delta t$ which gives the momentum at $n + 1$ as

$$\mathbf{p}_{(n+1)} = \mathbf{p}_{(n)} + q \Delta t \left[\mathbf{E}_{(n+1/2)} (\mathbf{x}_{(n+1/2)}) + \mathbf{x}_{(n+1/2)} \times \mathbf{B}_{(n+1/2)} (\mathbf{x}_{(n+1/2)}) \right] \quad (3.4)$$

where, the electric fields are extrapolated (?) to the intermediate point $n + 1/2$. Then, using $\mathbf{p} = \gamma m \mathbf{v}$, we can find the velocity at $n + 1$, from which we then have the current $\mathbf{J}_{(n+1)}$. We then reverse the order of computing such that the magnetic field is calculated prior to the electric field,

$$\mathbf{B}_{(n+1)} = \mathbf{B}_{(n+1/2)} - \frac{\Delta t}{2} \left(c^2 \nabla \times \mathbf{E}_{(n+1/2)} \right) \quad (3.5)$$

$$\mathbf{E}_{(n+1)} = \mathbf{E}_{(n+1/2)} + \frac{\Delta t}{2} \left(c^2 \nabla \times \mathbf{B}_{(n+1)} - \frac{\mathbf{J}_{(n+1)}}{\epsilon_0} \right) \quad (3.6)$$

Using these fields when then calculate the new particles positions $\mathbf{x}_{(n)}$, we "push" the particles, thus completing the iteration step.

3.3 EPOCH

The Extensible PIC Open Collaboration project (EPOCH) is an advance relativistic electromagnetic PIC code developed at the University of Warwick by XXX et al. [ref.user-manual]. EPOCH is now maintained and developed through the Collaborative Computational Project in Plasma Physics (CCP-Plasma), from which access to the code is granted to non-profit research laboratories and Universities [CCP website]. The underlying code is written in Fortran and allows for simulations to be run on multiple parallel processors via MPI; this enables time-consuming simulations to be run on remote computing clusters. The core PIC code in EPOCH is based upon the field update and particle push algorithms of the Plasma Simulation Code (PSC) written by H. Ruhl []. This follows closely the standard PIC method outline in section 3.2. The main difference being in how the FTDT method is implemented and the inclusion of additional functionality to allow for more advanced features such as collisions, ionisation and quantum electrodynamic radiation to be simulated [epoch manual]. EPOCH is highly user-friendly; setting up simulations simply requires users to specify the parameters and initial conditions of the simulations without the need to interact with the underlying PIC code. Likewise, analysing and visualising data from a simulations is made easier through file-compatibility with Python, Matlab, IDL and VisIt, the details of which will be covered in this section.

3.3.1 Input deck

Once EPOCH has been downloaded and compiled the so-called input deck is essentially EPOCH’s user interface. This is a file in which users specify the details of a simulations and it is this file that gets read by EPOCH and passed onto the core PIC algorithm. The input deck consists of blocks which define parameters for different features of the simulation.

Explain control block first, and what the restart does.

```
begin:control
  dlb_threshold = 0.5
  restart_snapshot=restartXXXX.sdf
  t_end = end_time
  nx = nint(length / cell_length)
  ny = nint((half_width * 2) / cell_width)
  npart = part_per_cell * nx * ny
  stdout_frequency = 50
  use_random_seed = T
end:control
```

This specifies the grid that the simulations is to run on. We then populate this grid with plasma particles. **Species block**, with explanation about analytical density distributions for plasma, and specify ppc.

The control and species blocks together define the resolution of the simulation. When setting up the resolution of the grid one has to make sure that the grid is sufficiently fine such that the smallest features of our physical system are resolved. This is to ensure that the simulation accurately models the physical system it is meant to represent, to the extent that missing small scale phenomena might alter the large scale outcome of the simulation. A finer grid however requires more macroparticles to fully populate the grid, which inevitably

extents the computational time. In addition the time step Δt needs to be suitably decreased as well. This is because of the so-called Courant-Friedrichs-Lowy (CFL) condition. Any simulation introduces uncertainties in the final outcome due to the finite resolution. We need to make sure that the uncertainties introduced during each iteration do not build up and grow unbounded.

edriver with analytical distribution, and laser, followed by boundaries

```
begin:boundaries
  bc_x_min = simple_laser
  bc_x_max = simple_outflow
  bc_y_min = simple_outflow
  bc_y_max = simple_outflow
end:boundaries
```

output block and the sdf file visualisation with VisIT

3.3.2 Non-analytical bunch initialisation

- Issue: restart not possible with laser.
- EPOCH allows for a user to manually override particle-parameter distributions defined in the input deck, in which all functions must be defined analytically. By overriding this so-called autoloader, which takes the analytical distributions in the input deck and distributes the macro particles accordingly, this manual approach allows for the initialisation of a bunch with non-analytical density and momentum distributions.
- Furthermore, even if the density distribution were to be easily described analytically, this method offers the advantage that it also overrides the maxwellian velocity distribution that epoch assigns to each bunch of particles in the input deck. This is fine for an initial bunch in thermal equilibrium, but as soon as plasma interaction occurs the velocity distribution of the electrons in the bunch is noticeably non-maxwellian
- VisIt - export data from .sdf file, convert to -csv, read with ic module when compiling epoch.
- (show below, it is possible to have a laser appear before the bunch at some time t, but the parameters of this laser could not be changed so testing several different laser intensities, distances etc. would take far too long if the bunch was forced to propagate 20cm each time before the laser was ramped up)

```

ExportDBAtts = ExportDBAttributes()
ExportDBAtts.allTimes = 0
ExportDBAtts.dirname = "/Users/oscarjakobsson/Documents/epoch-4.14.4/epoch2d"
ExportDBAtts.filename = "test"
ExportDBAtts.timeStateFormat = "%04d"
ExportDBAtts.db_type = "Xmdv"
ExportDBAtts.db_type_fullname = "Xmdv_1.0"
ExportDBAtts.variables = ("Particles/Ek/edriver", "Particles/Weight/edriver")
ExportDBAtts.writeUsingGroups = 0
ExportDBAtts.groupSize = 48
ExportDBAtts.opts.types = (0)
ExportDBAtts.opts.help = ""
ExportDatabase(ExportDBAtts)
ExportDBAtts = ExportDBAttributes()
ExportDBAtts.allTimes = 0
ExportDBAtts.dirname = "/Users/oscarjakobsson/Documents/epoch-4.14.4/epoch2d"
ExportDBAtts.filename = "test"
ExportDBAtts.timeStateFormat = "%04d"
ExportDBAtts.db_type = "Xmdv"
ExportDBAtts.db_type_fullname = "Xmdv_1.0"
ExportDBAtts.variables = ("Particles/Ek/edriver", "Particles/Weight/edriver")
ExportDBAtts.writeUsingGroups = 0
ExportDBAtts.groupSize = 48
ExportDBAtts.opts.types = (0)
ExportDBAtts.opts.help = ""
ExportDatabase(ExportDBAtts)

```

3.4 Notes.

Meeting Guoxing:

- We will change $\sigma_{x,y}$, in simulation from $\sigma_{x,y} = 0.3\mu m \rightarrow 5 - 10\mu m$ because the $0.3\mu m$ EuPRAXIA beam parameter gives to high beam density n_b , which means that we can't have $n_b \sim n_p$ because the plasma density would have to be too high. We should aim for $n_p \sim 10^{17} - 10^{18} \sim n_b$ (standard L/PWFA) parameters. EuPRAXIA wants $\sigma_{x,y}$ small because small bunches gives more coherent radiation in undulators. One could expand the beam by letting it propagate freely (expand due to space charge) a distance before reaching the beam dump.

- Run simulations with uniform plasma density for n_p :

$n_p \sim 0.1n_b$	Non-linear
$n_p \sim n_b$	Quasi-linear
$n_p \sim 10n_b$	Linear
- Use $\Delta E/E = 0.01$ and bunch charge 30 pC (5 fs).
- Estimate necessary simulation propagation length by saturation length using wave-

3. Simulations

breaking electric field gradient

$$L_{\text{sat}} \approx \frac{T_0}{eE_{\text{wb}}} = \frac{T_0}{e} \frac{e}{m_e c \omega_p} = \frac{T_0}{m_e c} \sqrt{\frac{m_e e \epsilon_0}{e^2 n_b}}$$

- Project outline:
 - Uniform plasma with varying $n_b \sim n_p$
 - Vary plasma density profile
 - Test laser to dump head of beam
 - Run simulations for real FlashForward parameters and not the idealized Eu-PRAXIA parameters.

- 100pC

$$n_b = \frac{N_p}{(2\pi)^{3/2} \sigma_y^2 \sigma_x^2} = \frac{6.25 \times 10^8}{(2\pi)^{3/2} (5 \times 10^{-6})^3} \approx 3.2 \times 10^{23} \text{ m}^{-3}$$

$$\Rightarrow eE_{\text{wb}} = \begin{cases} 17 \text{ GeV/m} & n_p = 0.1 n_b \\ 54 \text{ GeV/m} & n_p = n_b \\ 172 \text{ GeV/m} & n_p = 10 n_b \end{cases} \Rightarrow L_{\text{sat}}(1 \text{ GeV}) = \begin{cases} 5.8 \text{ cm} & n_p = 0.1 n_b \\ 1.9 \text{ cm} & n_p = n_b \\ 0.6 \text{ cm} & n_p = 10 n_b \end{cases}$$

$$1 \text{ GeV beam} \Rightarrow L_{\text{sat}} \sim 2 \text{ cm} = 2 * 10^4 \mu\text{m}$$

- 30pC

$$n_b = \frac{N_p}{(2\pi)^{3/2} \sigma_y^2 \sigma_x^2} = \frac{1.87 \times 10^8}{(2\pi)^{3/2} (5 \times 10^{-6})^3} \approx 9.5 \times 10^{22} \text{ m}^{-3}$$

$$\Rightarrow eE_{\text{wb}} = \begin{cases} 9.4 \text{ GeV/m} & n_p = 0.1 n_b \\ 30 \text{ GeV/m} & n_p = n_b \\ 94 \text{ GeV/m} & n_p = 10 n_b \end{cases} \Rightarrow L_{\text{sat}}(1 \text{ GeV}) = \begin{cases} 10.7 \text{ cm} & n_p = 0.1 n_b \\ 3.4 \text{ cm} & n_p = n_b \\ 1.1 \text{ cm} & n_p = 10 n_b \end{cases}$$

$$1 \text{ GeV beam} \Rightarrow L_{\text{sat}} \sim 3.4 \text{ cm} = 3.4 * 10^4 \mu\text{m}$$

4

Simulation tests

4.1 Plasma deceleration - Uniform density

4.1.1 Transverse instabilities in quasilinear regime

4.2 Hybrid Scheme - Feasibility study

4.2.1 Initialising a decelerated bunch

- Compare to actual already propagated bunch we want to simulate. See how quickly the uniform plasma resembles that of the plasma of the propagated simulation. If it takes long time then the laser results might not represent the real situation. Compare simulations side by side as both real and initialised bunches propagate further, see if any deviations occur or if the bunch I set up is actually a fair approximation (compare energy, particle number etc.)

4.2.2 Introduction of co-propagating laser

- Results with respect to laser intensity/amplitude/wavelength as well as distance from bunch.

4. Simulation tests

5

Ongoing and future work

Having constructed the necessary computational framework for simulating the hybrid beam dump scheme we can now investigate the feasibility of this scheme and proceed to work out the details of the bunch-laser interaction. This will include investigating and optimizing the distance at which the laser is introduced, the spatial separation between the bunch and the laser, the intensity and pulse length of the laser and effects caused by the difference in phase velocity between the bunch and the laser.

Once the details of the hybrid scheme has been investigated and a desirable approach has been determined we should proceed by high resolution simulations to verify that that the scheme works. As we have seen in section XXX the effect of insufficiently high simulation resolution can yield wildly different outcomes, as small effects can become amplified or neglected, in comparison to higher resolution runs. Consequently, in order to obtain reliable results from our simulations it is crucial to investigate the parameters that determine the resolution of the simulation. These include:

- The number of grid points: where a finer grid will increase the spatial resolution by having the macro-particles in adjacent grid cells be closer together, thus allowing the distribution of the plasma and bunch electrons to be more accurately modelled. This however comes at the cost of longer computational time.
- The number of macro particles in each grid cell: this has the same effect as using a finer grid by allowing the contents of grid cells to more accurately describe the distribution of micro-particles in those cells, since if only one macroparticle was used in a cell with electrons of varying energy and momentum that macroparticle would have to average these properties and thus remove the finer details of the plasma and bunch.
- The number of macro particles in the electron bunch: This number is crucial to accurately capture the small-scale effects on the bunch caused by the interaction with the plasma electrons.

How to establish these simulation parameters?

5. Ongoing and future work

We may divide the work on the hybrid scheme into three broad areas.

- Energy loss w.r.t bunch and plasma parameters
 - Eloss(bean width)
 - Eloss(length)
 - Eloss(n_p/n_b), where $n_p = n_p(\text{beam width, beam length})$
- Simulation parameters
 - Grid settings and resolution to avoid transverse instabilities
 - Minimise numerical noise using laser ramp
 - Accuracy vs. Computational cost
- Laser driver
 - Optimise laser parameters
 - * Time when introduced in simulation (at/before saturation)
 - * Distance from bunch
 - * Pulse length
 - * Intensity, wavelength
 - * Laser ramp
 - Further laser investigations
 - * Multiple consecutive laser pulses

6

Conclusion

Lorem ipsum dolor sit amet, consectetur adipisicing elit, sed do eiusmod tempor incididunt ut labore et dolore magna aliqua. Ut enim ad minim veniam, quis nostrud exercitation ullamco laboris nisi ut aliquip ex ea commodo consequat. Duis aute irure dolor in reprehenderit in voluptate velit esse cillum dolore eu fugiat nulla pariatur. Excepteur sint occaecat cupidatat non proident, sunt in culpa qui officia deserunt mollit anim id est laborum.

6. Conclusion

Bibliography

- [1] The Technical Design Report (TDR) of the European XFEL.
- [2] G Schrgder, U Jansson, R Jung, G R Stevenson, and E B Vossenberg. The LEP Beam Dumping System. pages 2429–2431.
- [3] Polepalle Satyamurthy, Pravin Rai, Vikas Tiwari, Kiran Kulkarni, John Amann, Raymond G. Arnold, Dieter Walz, Andrei Seryi, Tristan Davenne, Ottone Caretta, Chris Densham, and Robert B. Appleby. Design of an 18 MW vortex flow water beam dump for 500 GeV electrons/positrons of an international linear collider. *Nuclear Instruments and Methods in Physics Research, Section A: Accelerators, Spectrometers, Detectors and Associated Equipment*, 679:67–81, 2012.
- [4] H. C. Wu, T. Tajima, D. Habs, A. W. Chao, and J. Meyer-ter Vehn. Collective deceleration: Toward a compact beam dump. *Physical Review Special Topics - Accelerators and Beams*, 13(10):1–8, 2010.
- [5] A. Bonatto, C. B. Schroeder, J. L. Vay, C. G.R. Geddes, C. Benedetti, E. Esarey, and W. P. Leemans. Passive and active plasma deceleration for the compact disposal of electron beams. *Physics of Plasmas*, 22(8), 2015.
- [6] Kieran Hanahoe, Guoxing Xia, Mohammad Islam, Yangmei Li, Öznur Mete-Apsimon, Bernhard Hidding, and Jonathan Smith. Simulation study of a passive plasma beam dump using varying plasma density. *Physics of Plasmas*, 24(2), 2017.
- [7] John David Jackson. Jackson - Classical Electrodynamics (3rd Ed.).pdf, 1962.
- [8] T Katsouleas, S Wilks, P Chen, J M Dawson, and J J Su. BEAM LOADING IN PLASMA ACCELERATORS. Technical report, 1987.
- [9] S Vaganian and H Henke. THE PANOFSKY-WENZEL THEOREM AND GENERAL RELATIONS FOR THE WAKE POTENTIAL. Technical report, 1995.
- [10] John M Dawson. Electron Oscillations in a Cold Plasma. Technical Report 2, 1959.
- [11] W. Lu, C. Huang, M. Zhou, M. Tzoufras, F. S. Tsung, W. B. Mori, and T. Katsouleas. A nonlinear theory for multidimensional relativistic plasma wave wakefields. *Physics of Plasmas*, 13(5), 2006.
- [12] A. Bonatto, C. B. Schroeder, J. L. Vay, C. R. Geddes, C. Benedetti, E. Esarey, and W. P. Leemans. Compact disposal of high-energy electron beams using passive or laser-driven plasma decelerating stage. *AIP Conference Proceedings*, 1777(1):0–5, 2016.

Bibliography

A

Appendix: Input decks